

A systematic investigation of T-stresses for a variety of center-cracked tension specimens

メタデータ	言語: English 出版者: 公開日: 2015-05-14 キーワード (Ja): キーワード (En): 作成者: Lu, Kai, Meshii, Toshiyuki メールアドレス: 所属:
URL	http://hdl.handle.net/10098/8794

Accepted Manuscript

A systematic investigation of T -stresses for a variety of center-cracked tension specimens

Kai Lu, Toshiyuki Meshii

PII: S0167-8442(14)20106-6

DOI: <http://dx.doi.org/10.1016/j.tafmec.2015.02.001>

Reference: TAFMEC 1566

To appear in: *Theoretical and Applied Fracture Mechanics*



Please cite this article as: K. Lu, T. Meshii, A systematic investigation of T -stresses for a variety of center-cracked tension specimens, *Theoretical and Applied Fracture Mechanics* (2015), doi: <http://dx.doi.org/10.1016/j.tafmec.2015.02.001>

This is a PDF file of an unedited manuscript that has been accepted for publication. As a service to our customers we are providing this early version of the manuscript. The manuscript will undergo copyediting, typesetting, and review of the resulting proof before it is published in its final form. Please note that during the production process errors may be discovered which could affect the content, and all legal disclaimers that apply to the journal pertain.

A systematic investigation of T -stresses for a variety of center-cracked tension specimens

Kai Lu^{a*}, kai_lu@u-fukui.ac.jp, Toshiyuki Meshii^b

^aGraduate School of Engineering, University of Fukui, 3-9-1 Bunkyo, Fukui, Fukui, Japan

^bFaculty of Engineering, University of Fukui, 3-9-1 Bunkyo, Fukui, Fukui, Japan

*Corresponding author. Fax: +81 776 27 9764.

Abstract

In this work, a systematic investigation of three-dimensional (3D) T -stresses (T_{11} and T_{33}) was conducted using detailed elastic finite element analysis (FEA). The interaction integral method was applied to extract the T -stress solutions. Standard CCT specimens with a thickness-to-width ratio of $B/(2W) \leq 0.0625$ and a crack length-to-thickness ratio of $2a/B \geq 8$, as specified in ASTM E2472, were considered, and the cases of $B/(2W) = 0.1 \sim 1.0$ and $2a/B = 0.05 \sim 7$ were also added. From the FEA results, it was found that both T_{11} and T_{33} at the specimen mid-plane showed significant changes with crack lengths and specimen thicknesses for those CCT configurations that satisfy ASTM E2472. Because both the in-plane and out-of-plane T -stresses were negative and showed large variations for all the considered CCT specimens which was true even for the CCT specimens complying with the ASTM E2472 standard, it was noted that these CCT specimens that complying with the standard might show the test specimen size effect (including the crack length and specimen thickness effect) on the fracture toughness if tested.

Keywords:

T -stresses, Center-cracked specimen, Constraint effect, Finite element analysis, Fracture toughness

Nomenclature

B	Specimen thickness
E	Young's modulus
H	Half specimen height
I	Interaction integral
J_c	Fracture toughness of a material in the ductile-to-brittle transition temperature region
K_I	Local mode I stress intensity factor
R_s	Crack tube radius
T_{11}, T_{33}	T -stresses obtained from the finite element analysis results
$T_{11 \text{ sup}}, T_{33 \text{ sup}}$	T -stresses obtained from the superposition method
W	Half specimen width
W_{\min}	Minimum half specimen width
a	Half crack length
f	Unit magnitude (see Eq. (2))
r, θ	In-plane polar coordinates
x_j	Crack-tip local coordinates ($j = 1, 2, 3$)
Δ	Singular element size
V_{11}, V_{33}	Normalized T -stresses from the finite element analysis results
$V_{11 \text{ Kfour}}^{\text{Kfour}}$	Normalized Kfour's plane strain T_{11} solutions
$V_{11 \text{ sup}}, V_{33 \text{ sup}}$	Normalized T -stresses obtained from the superposition method
ε_3	Out-of-plane strain
ν	Poisson's ratio
σ	Uniform tension load
σ_{ij}	Stress components ($i, j = 1, 2, 3$)

1. Introduction

The crack-tip constraint difference caused by the specimen configuration and the size of fracture test specimens is known to show a strong effect on the measured fracture toughness [1, 2]. The past fracture toughness test results [3-5] indicated two common understandings, that is, (1) a high level of crack-tip constraint results in low fracture toughness, while a low constraint leads to a higher fracture toughness; (2) the change in the measured fracture toughness is small for a high constraint case but the fracture toughness is sensitive for a low constraint case. Therefore, the center-cracked tension (CCT) specimen in Fig. 1, which is considered to be a representative of the low constraint specimen [6, 7], should be sensitive to the constraint difference caused by specimen size difference [3, 8, 9], if there is any. The past fracture toughness test results for the various sized CCT specimens [10] seemed to validate this sensitivity. Thus, studies on the crack-tip constraint difference for various sized CCT specimens were thought to be necessary. As a parameter to quantify the crack-tip constraint, the elastic T -stresses were considered [11].

The in-plane T -stress, T_{11} , which is thought to be a measure of the in-plane crack-tip constraint, has been extensively investigated in the previous works for various fracture toughness test specimens and cracked structures [7, 12-25].

In discussing the CCT specimens, six T_{11} solutions in two-dimension (2D) [7, 13, 16, 19, 22, 24] and one in three-dimensions (3D) [24] are known. Five of them used the finite element method [7, 13, 19, 24], one of them used the boundary collocation method [16] and the other used the boundary element method [22]. In these six 2D works, five presented T_{11} solutions for the plane strain condition [7, 13, 19, 22, 24] and one for the plane stress condition [16]. Among these five plane-strain T_{11} solutions, Kfoury [13] and Tan and Wang's solutions [22] were obtained for isotropic materials with Poisson's ratio $\nu = 0.3$. The difference in these two solutions was that Kfoury's solutions [13] covered the crack length-to-width ratio $a/W = 0.1-0.6$, while Tan and Wang [22] covered $a/W = 0.2-0.6$. The third plane strain T_{11} solutions by Paulino and Kim [7] were obtained for both homogeneous and functionally graded materials. In case of a homogeneous material, they assumed $\nu = 0.3$ and considered cases for $a/W = 0.1-0.8$. The fourth plane strain T_{11} solutions by Henry and Luxmoore [24] were obtained for $a/W = 0.1-0.9$, assuming a homogeneous material of $\nu = 0.33$. The remaining one plane strain T_{11} solutions by Shlyannikov [19] added cases for inclined cracks (mixed-mode loading), assuming a homogeneous material of $\nu = 0.3$. The T_{11} solutions presented for a non-inclined crack were for the cases $a/W = 0.1-0.9$. The only plane stress T_{11} solutions by Fett [16] were obtained for a homogeneous material of $\nu = 0.25$ and for $a/W = 0 - 1.0$. In addition to the effect of a/W on T_{11} , he also examined the effect of H/W in the range of $0.35 - 1.25$. In addition to the above six 2D works, T_{11} solutions of 2D CCT specimens were also provided in some benchmark analyses (e.g., Chen and Wang [23]). Although various 2D T_{11} solutions are available for CCT specimens, to the best of our knowledge, the 3D T_{11} solutions of the CCT specimens can only be

found in Henry and Luxmoore's paper [24], assuming a homogeneous material of $\nu = 0.33$ and for the specific case of a thickness-to-width ratio $B/(2W)$ of 0.25. The planar size effect of $a/W = 0.1-0.9$ was investigated. In addition to the results for $\nu = 0.33$, the effect of Poisson's ratio ($\nu = 0 \sim 0.495$) was also investigated for the case of $a/W = 0.7$. Although they noted out the existence of the 3D effect by comparing the 2D plane-strain T_{11} with the 3D solutions, the out-of-plane T -stress, T_{33} [11, 18, 20, 26-32], which is thought to be a measure of the out-of-plane crack-tip constraint, has not been studied for the CCT specimens. Thus, in this work, a systematic investigation of the 3D T -stresses (T_{11} and T_{33}) for a variety of CCT specimens was conducted by using 3D elastic finite element analysis (FEA).

For that purpose, the standard CCT specimens, as specified in ASTM E2472 [33], with a minimum half specimen width of $W_{\min} \geq 150$ mm, a specimen height-to-width ratio of $H/W \geq 1.5$, a thickness-to-width ratio of $B/(2W) \leq 0.0625$ and a crack length-to-thickness ratio of $2a/B \geq 8$ were investigated. In addition, the cases of $B/(2W) = 0.1 \sim 1.0$ and $2a/B = 0.05 \sim 7$ were added to the systematic investigation.

Based on the FEA results, it was found that the 3D in-plane T_{11} at the specimen mid-plane was a monotonously decreasing function of the crack length when $a/W \geq 0.3$ and showed a slight change with the crack length when $a/W < 0.3$. Another finding was that the mid-plane T_{11} showed a variation as high as 22% in the range of $B/(2W) = 0.01$ to 0.0625 at $a/W = 0.5$, even though these $B/(2W)$ ratios satisfy ASTM E2472 [33]. The newly obtained mid-plane T_{33} was negative for all of the cases considered. The mid-plane T_{33} was a monotonously increasing function of the specimen thickness. In particular, T_{33} showed a significant change for the cases of $B/(2W) \leq 0.0625$ and $2a/B \geq 8$, even for those configurations that satisfy ASTM E2472 [33]. Because both the in-plane and out-of-plane T -stresses were negative for the CCT specimens and showed large variations for all the considered CCT specimens which is true even for cases complying with the standard ASTM E2472 [33], it was noted that these CCT specimens that complying with the standard might show the test specimen size effect (including the crack length and specimen thickness effect) on the fracture toughness if tested.

Fig. 1. CCT specimen

2. T -stress

In an isotropic and linear elastic 3D body containing a crack subjected to symmetric (mode I) loading, the leading two terms in the Williams series expansion [34] of the crack-tip stress fields near the crack front can be written as follows [14]:

$$\begin{pmatrix} \sigma_{11} \\ \sigma_{22} \\ \sigma_{33} \\ \sigma_{12} \\ \sigma_{23} \\ \sigma_{31} \end{pmatrix} = \frac{K_I}{\sqrt{2\pi r}} \begin{pmatrix} \cos \frac{\theta}{2} \left(1 - \sin \frac{\theta}{2} \sin \frac{3\theta}{2}\right) \\ \cos \frac{\theta}{2} \left(1 + \sin \frac{\theta}{2} \sin \frac{3\theta}{2}\right) \\ 2\nu \cos \frac{\theta}{2} \\ \sin \frac{\theta}{2} \cos \frac{\theta}{2} \cos \frac{3\theta}{2} \\ 0 \\ 0 \end{pmatrix} + \begin{pmatrix} T_{11} \\ 0 \\ T_{33} \\ 0 \\ 0 \\ 0 \end{pmatrix} \quad (1)$$

where r and θ are the in-plane polar coordinates of the plane normal to the crack front shown in Fig. 2 [28, 32], K_I is the local mode I stress intensity factor (SIF) and ν is Poisson's ratio. Here, x_1 is the direction formed by the intersection of the plane normal to the crack front and the crack plane. T_{11} and T_{33} are the amplitudes of the second-order terms in the three-dimensional series expansions of the crack front stress field in the x_1 and x_3 directions, respectively.

Fig. 2 Three-dimensional coordinate system for the region along the crack front [28, 32]

Several methods have been proposed to evaluate the elastic T -stresses for different cracked geometries in recent studies. Sherry et al. [15] gave a brief summary of the different methods used for calculating the in-plane T -stress T_{11} . Based on the works by Cardew et al. [12] and Kfoury [13], Nakamura and Parks [14] developed an interaction integral method to extract the elastic T_{11} for 3D mode I crack problems with the related calculation of the crack-tip T_{11} on the crack front as:

$$T_{11} = \frac{E}{1-\nu^2} \left\{ \frac{I}{f} + \nu \varepsilon_{33} \right\} \quad (2)$$

where E denotes Young's modulus, ν is Poisson's ratio and ε_{33} represents the out-of-plane strain at the crack-tip in the direction tangential to the crack front. I represents the interaction integral, and f indicates the unit magnitude ($f = 1$). In Eq. (2), it should be noted that, for a specified material, the in-plane T_{11} will be affected by not only the interaction integral I but also the out-of-plane strain ε_{33} .

For a 3D cracked problem, in addition to the in-plane T_{11} , Nakamura and Parks [14] were the first to define the relationship for determining the out-of-plane T -stress T_{33} :

$$T_{33} = E \varepsilon_{33} + \nu T_{11} \quad (3)$$

According to Eq. (3), it is clear that the out-of-plane T_{33} naturally depends on the out-of-plane strain ε_{33} and inevitably shows its dependence on the in-plane T_{11} .

More details of the interaction integral method can be found in Nakamura and Parks [14].

3. Finite Element Analysis

3.1 Details of the elastic FEA

Our interest was focused on the influence of 3D effects on various CCT specimens. Thus, the 3D

elastic FEA was run to calculate the elastic T -stresses (T_{11} and T_{33}) for different CCT specimens. The FEA model was configured with a through-thickness straight crack, as shown in Fig. 3(a). For all of the cases in the present FEA, the specimen width and specimen height was fixed as $2W = 300$ mm and $2H = 600$ mm, respectively. The set W and H satisfy the size requirements specified in ASTM E2472 [33] of $W_{\min} \geq 150$ mm, and $H/W \geq 1.5$. $H = 2W$ was selected because the numerical results were reported as being slightly affected by the specimen height [13, 35, 36] and because this value has been used as a guideline for many years [37].

To study the 3D T -stresses (T_{11} and T_{33}) for a variety of CCT specimens, the ASTM E2472 [33] standard CCT specimens with a thickness-to-width ratio $B/(2W) \leq 0.0625$ and a crack length-to-thickness ratio $2a/B \geq 8$ were investigated. In addition, the cases of $B/(2W) = 0.1 \sim 1.0$ and $2a/B = 0.05 \sim 7$ were added to the systematic investigation.

Considering the symmetry conditions of the CCT specimens (Fig. 3(a)), the 1/8 symmetric model was built using the software FEA Crack [38], as shown in Fig. 3(b). The finite element model was generated using twenty-node isoparametric 3D solid elements with reduced ($2 \times 2 \times 2$) Gauss integration. Sixteen singular elements were always used around the crack-tip throughout the calculations. A constant crack tube radius, $R_s = 1.0$ mm, was set with twenty equivalent rings spaced inside it (Fig. 3(c)). The smallest element size Δ relative to the crack length in the created models was in the range of $(0.42 \sim 6.7) \times 10^{-3}$, as summarized in Table A.1. For the present FEA models, 78,720 to 93,632 elements with a total of 332,459 to 393,141 nodes were generated. The detailed mesh generation information is summarized in the Appendix.

The material is assumed to be isotropic and linearly elastic. The Young's modulus $E = 206$ GPa and Poisson's ratio $\nu = 0.3$ were adopted in the present FEA.

Because of the symmetry conditions (Fig. 3(a)), the displacements normal to the symmetry planes of the 1/8 symmetric FEA model were fixed, and they are grey-colored in Fig. 3(b). In applying a remote tensile loading, a uniform stress $\sigma = 1$ MPa was applied on the remote plane $x_2 = H$ at the far-end of the model.

WARP3D [39] was used as the FEA solver.

Fig. 3 Typical 1/8 symmetric finite element model of a CCT specimen ($2W = 300$ mm, $H/W = 2$, $B/(2W) = 0.5$ and $a/W = 0.5$). Note that the detailed information for the mesh generation parameters (Δ , CD, NR and na) is summarized in the Appendix.

3.2 Validation of the evaluated T -stresses

For all current FEAs, the T -stress results were evaluated by taking the average values obtained from domain 2 to domain 20 (domain m consists of the elements from the 1st ring to the m^{th} ring). T values were found to be independent on the chosen domains, as the differences in the T -stress results

from domain 2 to domain 20 were within 0.1% of each other. We focused our attention on the specimen mid-plane T -stresses under the assumption that fracture initiation occurs at this location (e.g., [10, 27, 28]), and reported the T -stress solutions in the normalized form of $V_{kk} = T_{kk}/\sigma$ ($k = 1$ or 3).

Before summarizing the various T -stress solutions for CCT specimens with large crack length and thickness variations, the FEA model and evaluated T -stresses are validated in two steps. First, our 3D T_{11} solutions at the specimen mid-plane for the thickest specimen of $B/(2W) = 1.0$ were compared with Kfourri's 2D plane strain T_{11} solutions [13]. This ratio, $B/(2W) = 1.0$, was selected to confirm whether the 3D T_{11} solutions might approach the plane strain values for a large thickness even though $B/(2W) = 1.0$ ($B = 300$ mm) might not be realistic for a CCT specimen. Note that Kfourri's plane strain solutions [13] are only available for $a/W = 0.1$ to 0.6.

In Fig. 4 and Table 1, the present mid-plane V_{11} solutions show a relatively large difference compared with Kfourri's solutions, $V_{11 \text{ Kfourri}}$ [13] as 5.4% for $a/W = 0.5$ and 9.5% for $a/W = 0.6$. When comparing the present mid-plane V_{11} solutions for $B/(2W) = 0.5$ and 1.0 as summarized later in Table 2, it is found that the present V_{11} solutions have not shown the saturating tendency for $B/(2W) = 1.0$. Moreover, for a thick specimen with $B/(2W) \geq 0.5$, the difference between the present V_{11} solutions and Kfourri's solutions [13] increases. This result indicates that the stress state for a CCT specimen with a large thickness may deviate from the plane strain condition, which seems to contradict the common understanding that a thick specimen approaches the plane strain condition. Thus, we proceeded to the second step for T -stress validations.

Fig. 4 Comparison of the normalized 3D mid-plane T_{11} solutions ($V_{11} = T_{11}/\sigma$) with Kfourri's 2D plane strain solutions [13] and the solutions from the superposition method for the CCT specimens with $B/(2W) = 1.0$ ($\nu = 0.3$)

The second step was to apply the superposition method for T_{11} [18] and T_{33} [31] in this work for validation. For example, in the case of $B/(2W) = 1.0$, the normalized mid-plane T -stress solutions from the superposition method (designated as $V_{11 \text{ sup}}$ and $V_{33 \text{ sup}}$) were compared with the mid-plane V_{11} and V_{33} solutions from the present FEA, as summarized in Table 1. It is clear from Table 1 that the maximum difference of the mid-plane V_{11} and $V_{11 \text{ sup}}$ solutions is 0.03% and the maximum difference for the mid-plane V_{33} and $V_{33 \text{ sup}}$ solutions is 0.16%.

Although only one validation example of $B/(2W) = 1.0$ is presented in this paper, the validations for the other CCT models have also been confirmed. Considering all cases, the maximum difference for the mid-plane V_{11} and $V_{11 \text{ sup}}$ solutions is 0.03% and the maximum difference for the mid-plane V_{33} and $V_{33 \text{ sup}}$ solutions is 0.40%. Thus, it is concluded that the present FEA models were suitable and that the obtained T -stress solutions have sufficient accuracy.

Table 1 Comparisons of the mid-plane normalized T -stress results for CCT specimens from the present FEA and the superposition method ($2W = 300$ mm, $H/W = 2$, $B/(2W) = 1.0$; $\nu = 0.3$)

3.3 T -stress solutions for CCT specimens

Next, the normalized mid-plane V_{11} values for all of the cases in the present FEA are summarized as shown in Table 2 and Fig. 5. Note that the mid-plane V_{11} is always negative for all cases.

In Fig. 5, regardless of $B/(2W)$, the mid-plane V_{11} is a monotonously decreasing function of the crack length for $a/W \geq 0.3$, but it changes slightly for $a/W < 0.3$, which is similar to Kfoury's 2D plane strain solutions [13]. Considering the ASTM E2472 [33] standard CCT specimens with $B/(2W) \leq 0.0625$ and $2a/B \geq 8$, it is observed that the mid-plane V_{11} shows a relatively small dependence on the crack length for $a/W \leq 0.5$, which satisfies the ASTM E2472 standard [33], and this result indicates that the a/W specification in ASTM E2472 [33] is appropriate. Conversely, the mid-plane V_{11} decreases significantly with the crack length for the CCT specimens with $a/W > 0.5$. Similar results were also obtained by Henry and Luxmoore [24] and Shlyannikov [19] for the CCT specimens. The sudden decrease in V_{11} for $a/W > 0.5$ seems to mean that the in-plane crack-tip constraint will decrease for a CCT specimen with a deep crack, and this finding coincides with the past fracture toughness test results of the CCT specimens, which indicated that a higher J_c (J_c : fracture toughness of a material in the ductile-to-brittle transition temperature region) value is obtained for a CCT specimen with a deep crack than for a CCT specimen with a shallow crack [3, 40].

Although the T_{11} stress is thought to be an in-plane constraint parameter, it is clear from Fig. 5 that the mid-plane V_{11} also exhibits 3D effects, that is, the mid-plane V_{11} decreases with an increase in $B/(2W)$, regardless of a/W . A similar tendency was found by Nakamura and Parks for a single edge-cracked plate under tension [14] and during our recent experience with the SE(B) specimens [28]. As seen in Fig. 5, the mid-plane T_{11} showed a variation as high as 22% in the range of $B/(2W) = 0.01$ to 0.0625 at $a/W = 0.5$ even though this set of $B/(2W)$ and a/W satisfies ASTM E2472 [22].

Table 2 Normalized T_{11} solutions ($V_{11} = T_{11}/\sigma$) at the specimen mid-plane for CCT specimens ($\nu = 0.3$)

Fig. 5 Normalized T_{11} solutions ($V_{11} = T_{11}/\sigma$) at the specimen mid-plane for CCT specimens ($\nu = 0.3$)

Table 3 and Fig. 6 summarize the mid-plane V_{33} solutions for various thicknesses and crack depths. The newly obtained mid-plane T_{33} is negative for all of the cases considered. In Fig. 6, it is observed that V_{33} is a monotonously increasing function of $B/(2W)$, as expected. Specifically, T_{33} shows a significant change for the cases of $B/(2W) \leq 0.0625$ and $2a/B \geq 8$ ($a/W \leq 0.5$) even though

these configurations satisfy ASTM E2472 [33]. However, it is observed that the increase in V_{33} with $B/(2W)$ for $B/(2W) \leq 0.0625$ is smaller than that for $B/(2W) \geq 0.1$.

In summary, both the in-plane and out-of-plane T -stresses were negative and showed large variations for all the considered CCT specimens. This was true even for cases complying with the ASTM E2472 [33].

Table 3 Normalized T_{33} solutions ($V_{33} = T_{33}/\sigma$) at the specimen mid-plane for CCT specimens ($\nu = 0.3$)

Fig. 6 Normalized T_{33} solutions ($V_{33} = T_{33}/\sigma$) at the specimen mid-plane for CCT specimens ($\nu = 0.3$)

4. Discussion

Although the minimum thickness-to-width ratio $B/(2W) = 0.01$ might seem unrealistic, there is a fracture toughness test for a CCT specimen with $B/(2W) = 0.003$ reported in [10].

Because both the mid-plane T -stresses (T_{11} and T_{33}) were negative for the CCT specimens and showed large variations for all the considered CCT specimens, which was true even for cases complying with the ASTM E2472 [33], it was noted that these CCT specimens that complying with the standard might show the test specimen size effect (including the crack length and specimen thickness effect) on the fracture toughness if tested.

In addition to the mid-plane T -stress solutions, the variations of the normalized V_{11} and V_{33} solutions in the thickness direction along the crack front were studied for all cases. The similar tendency of the V_{11} and V_{33} distributions in the thickness direction for the CCT specimens with various thicknesses was obtained regardless of a/W . Here, an example case of $a/W = 0.5$ with various thicknesses is summarized in the following figures. Note that the mid-side node values from the FEA results were excluded. In these figures, $x_3 = 0$ represents the value at the specimen mid-plane and $x_3 = B/2$ corresponds to the value at the free surface.

As observed in Fig. 7, the normalized in-plane T_{11} (V_{11}) distributions in the specimen thickness direction show an overall non-negligible variation for most of the cases studied in this work. There might be an opinion that T_{11} in the thickness direction will show nearly no variation for a very thin specimen. However, considering the ASTM E2472 standard CCT specimens with $B/(2W) \leq 0.0625$, it is clear from Fig. 7 that the variation of V_{11} in the thickness direction increases visibly as $B/(2W)$ decreases and that the largest variation of the V_{11} distribution is observed as 16.5% for the thinnest specimen of $B/(2W) = 0.01$ in the range of $x_3/(B/2) = 0$ to 0.8. When $B/(2W) > 0.0625$, it is observed that the overall variation of the V_{11} distributions becomes small. However, for an extremely thick specimen of $B/(2W) = 1.0$ ($B = 300$ mm), which might be considered to be unrealistic, the variation of V_{11} in the thickness direction is also non-negligible, with a 9.5% variation observed in the range of

$x_3/(B/2) = 0$ to 0.8 . A similar tendency can be found for a thick SE(B) test specimen (the thickness-to-width ratio is two), as reported in our recent work [28].

Fig. 7 Normalized T_{11} solutions ($V_{11} = T_{11}/\sigma$) vs. $x_3/(B/2)$ for the CCT specimens with various thicknesses ($a/W = 0.5$; $\nu = 0.3$)

Conversely, the normalized out-of-plane T_{33} distributions in Fig. 8 decrease in the thickness direction, considering that the ordinate of this figure ranges from -4 to 0 . The decreasing tendency is more visible for the ASTM standard CCT specimens with $B/(2W) \leq 0.0625$, especially for the case of $B/(2W) = 0.01$, because the difference in V_{33} in the range of $x_3/(B/2) = 0$ to 0.8 is 76% . However, the rate of decrease in V_{33} becomes small as $B/(2W)$ increases, which is clear for the case of $B/(2W) = 1.0$ (the difference of V_{33} in the range of $x_3/(B/2) = 0$ to 0.8 is 31%). A similar result can be obtained for the SE(B) test specimen in our recent work [28].

Fig. 8 Normalized T_{33} solutions ($V_{33} = T_{33}/\sigma$) vs. $x_3/(B/2)$ for the CCT specimens with various thicknesses ($a/W = 0.5$; $\nu = 0.3$)

It should also be noted that both T_{11} and T_{33} diverge near the free surface ($x_3/(B/2) = 0.8$ to 1.0) because ξ_3 tends to be singular in the region close to the free surface and cannot be accurately calculated using the present FEA method [14, 28, 41]. Thus, the T -stresses near the free surface calculated by the present FEA method require further study.

In addition to the 3D effects on CCT's T -stresses presented in this paper, another remaining interest is the Poisson's ratio effect on the T -stresses. Among the seven prior works on CCT T -stresses, Henry and Luxmoore [24] were the only researchers who examined the effects of Poisson's ratio ν by obtaining the 3D mid-plane T_{11} solutions of CCT specimens for the case of $B/(2W) = 0.25$ and $a/W = 0.7$. From their results for $\nu = 0, 0.1, 0.2, 0.33, 0.4$ and 0.495 , they concluded that $T_{11} \propto \nu$. Let us see whether this is true and the same relationship is obtained for various thicknesses. Also of interest is the relationship between T_{33} and ν which was not presented by them.

Fig. 9(a) is a comparison of the present mid-plane V_{11} solutions of $B/(2W) = 0.25$ with Henry and Luxmoore's results obtained from both the boundary layer method (BLM) and the displacement field method (i.e., uniform displacement applied on the far end of the specimens) [24]. Although Henry and Luxmoore concluded that the relationship $T_{11} \propto \nu$ could be obtained from their results, it is clearly observed from Fig. 9(a) that their conclusion ($T_{11} \propto \nu$) seems to be a rough compilation and that, rigorously speaking, V_{11} was a monotonously increasing function of ν . The present results are close to their result according to BLM, which they noted to be more accurate. To conclude, V_{11} was a monotonously increasing function of ν which showed approximately 20% change in the range of $\nu = 0$ to

0.495.

Fig. 9(b) summarizes how the relationship in Fig. 9(a) changes due to specimen thickness. In concrete, the effects of ν ($\nu = 0.1, 0.3$ and 0.495) on the mid-plane V_{11} solutions for CCT specimens with $B/(2W) = 0.01, 0.0625, 0.25, 0.5$ and 1.0 , for a case of $a/W = 0.7$, were investigated. It is seen from Fig. 9 (b) that, although the mid-plane normalized T_{11} (V_{11}) solutions monotonously increase with ν the effect of ν on V_{11} is strengthened for thin specimens and becomes negligible for thick specimens. It is worth noting that the change in the mid-plane V_{11} with ν is not negligible for the ASTM standard specimens with $B/(2W) \leq 0.0625$. In summary, T_{11} solutions are more sensitive to Poisson's ratio for a thin CCT specimen than those for a thick CCT specimen.

Fig. 9 Effects of Poisson's ratio ν on the mid-plane V_{11} for the case of $a/W = 0.7$: (a) comparison of present V_{11} for $B/(2W) = 0.25$ with Henry and Luxmoore's results [24] (b) present V_{11} for various thicknesses

In addition to $a/W = 0.7$, Fig. 10(a) summarizes the effects of ν on the mid-plane V_{11} solutions for CCT specimens with $a/W = 0.5$ (standard in ASTM E2472 [33]), but of various thicknesses. In Fig. 10(a), the effects of ν on the mid-plane V_{11} of $a/W = 0.5$ are similar with those obtained for $a/W = 0.7$ as shown in Fig. 9(b). However, compared with the cases of $a/W = 0.7$, the change in the mid-plane V_{11} due to the increase in ν becomes smaller for $a/W = 0.5$. For an example case of $B/(2W) = 0.01$, the maximum difference of V_{11} between the cases for $\nu = 0.1$ and 0.495 was 394% for $a/W = 0.5$, while the difference was 441% for the case of $a/W = 0.7$.

In addition, Fig. 10(b) plots the effects of ν on the mid-plane V_{33} solutions for CCT specimens with a standard $a/W = 0.5$, but of various thicknesses. It is clear that the mid-plane V_{33} show a monotonously decreasing function of Poisson's ratio ν regardless of $B/(2W)$. The observed relationship was approximately linear, and this effect was larger compared with the cases of V_{11} . The relationship is expected from Eq. (3), in case of negative and constant V_{11} . Because T_{11} was a monotonously increasing function of V_{11} , this enhanced the effect of ν on V_{33} . The decrease in V_{33} is significant for the ASTM standard specimens with $B/(2W) \leq 0.0625$, and the maximum difference of V_{33} for $\nu = 0.1$ and 0.495 is very large (531%) for $B/(2W) = 0.01$, while the change in V_{33} becomes smaller as $B/(2W)$ increases, and the minimum difference of V_{33} for $\nu = 0.1$ and 0.495 is as large as 476% for $B/(2W) = 1.0$.

In summary, T_{11} and T_{33} are more sensitive to Poisson's ratio for a thin CCT specimen than those for a thick CCT specimen. The effects of Poisson's ratio on T_{11} and T_{33} become small as a/W decreases.

Fig. 10 Effects of Poisson's ratio ν on the mid-plane V_{11} and V_{33}
for a case of $a/W = 0.5$: (a) V_{11} vs. ν (b) V_{33} vs. ν

5. Conclusions

The present study conducted a systematic investigation of the 3D T -stresses (T_{11} and T_{33}) for a variety of CCT specimens by running 3D elastic FEA. The conclusions obtained from this work are summarized as follows:

- (1) Both the mid-plane T_{11} and T_{33} were negative for the CCT specimens considered in this study.
- (2) The 3D in-plane T_{11} at the specimen mid-plane was a monotonously decreasing function of the crack length at $a/W \geq 0.3$ and showed a slight change with the crack length at $a/W < 0.3$.
- (3) The mid-plane T_{11} showed a variation as high as 22% in the range of $B/(2W) = 0.01$ to 0.0625 at $a/W = 0.5$, even though these $B/(2W)$ ratios that satisfy ASTM E2472.
- (4) The newly obtained mid-plane T_{33} was a monotonously increasing function of the specimen thickness. In particular, T_{33} showed a significant change for the cases of $B/(2W) \leq 0.0625$ and $2a/B \geq 8$, even though these configurations satisfy ASTM E2472.

Acknowledgements

This work was supported in part by JSPS KAKENHI Grant Number 24561038. Their support is greatly appreciated.

Appendix

The detailed information of the mesh generation parameters is given in Table A.1. Please refer to Fig. 3 for the definitions of the mesh generation parameters Δ , CD, NR and n_a .

Table A.1 Summary of the detailed mesh generation (NE: number of elements)

ACCEPTED MANUSCRIPT

List of figures

Fig. 1 CCT specimen

Fig. 2 Three-dimensional coordinate system for the region along the crack front [28, 32]

Fig. 3. Typical 1/8 symmetric finite element model of a CCT specimen ($2W = 300$ mm, $H/W = 2$, $B/(2W) = 0.5$ and $a/W = 0.5$). Note that the detailed information for the mesh generation parameters (Δ , CD, NR and na) is summarized in the Appendix.

Fig. 4 Comparison of the normalized 3D mid-plane T_{11} solutions ($V_{11} = T_{11}/\sigma$) with Kfourri's 2D plane strain solutions [13] and the solutions from the superposition method for the CCT specimens with $B/(2W) = 1.0$ ($\nu = 0.3$)

Fig. 5 Normalized T_{11} solutions ($V_{11} = T_{11}/\sigma$) at the specimen mid-plane for CCT specimens ($\nu = 0.3$)

Fig. 6 Normalized T_{33} solutions ($V_{33} = T_{33}/\sigma$) at the specimen mid-plane for CCT specimens ($\nu = 0.3$)

Fig. 7 Normalized T_{11} solutions ($V_{11} = T_{11}/\sigma$) vs. $x_3/(B/2)$ for the CCT specimens with various thicknesses ($a/W = 0.5$; $\nu = 0.3$)

Fig. 8 Normalized T_{33} solutions ($V_{33} = T_{33}/\sigma$) vs. $x_3/(B/2)$ for the CCT specimens with various thicknesses ($a/W = 0.5$; $\nu = 0.3$)

Fig. 9 Effects of Poisson's ratio ν on the mid-plane V_{11} for the case of $a/W = 0.7$: (a) comparison of present V_{11} for $B/(2W) = 0.25$ with Henry and Luxmoore's results [24] (b) present V_{11} for various thicknesses

Fig. 10 Effects of Poisson's ratio ν on the mid-plane V_{11} and V_{33} for a case of $a/W = 0.5$: (a) V_{11} vs. ν (b) V_{33} vs. ν

List of tables

Table 1 Comparisons of the mid-plane normalized T -stress results for CCT specimens from the present FEA and the superposition method ($2W = 300$ mm, $H/W = 2$, $B/(2W) = 1.0$; $\nu = 0.3$)

Table 2 Normalized T_{11} solutions ($V_{11} = T_{11}/\sigma$) at the specimen mid-plane for CCT specimens ($\nu = 0.3$)

Table 3 Normalized T_{33} solutions ($V_{33} = T_{33}/\sigma$) at the specimen mid-plane for CCT specimens ($\nu = 0.3$)

Table A.1 Summary of the detailed mesh generation (NE: number of elements)

ACCEPTED MANUSCRIPT

References

- [1] X. K. Zhu, J.A. Joyce, Review of fracture toughness (G, K, J, CTOD, CTOA) testing and standardization, *Engineering Fracture Mechanics* 85 (2012) 1-46.
- [2] V.N. Shlyannikov, N.V. Boychenko, A.M. Tartygasheva, In-plane and out-of-plane crack-tip constraint effects under biaxial nonlinear deformation, *Engineering Fracture Mechanics* 78 (2011) 1771-1783.
- [3] J.D.G. Sumpter, A.T. Forbes, Constraint based analysis of shallow cracks in mild steel, *Proceedings of TWI/EWI/IS International Conference on Shallow Crack Fracture Mechanics Test and Applications*, Cambridge, UK, 23-24 September, 1992.
- [4] W.A. Sorem, R.H. Dodds, S.T. Rolfe, Effects of crack depth on elastic-plastic fracture toughness, *International Journal of Fracture* 47 (1991) 105-126.
- [5] M.T. Kirk, R.H. Dodds, The influence of weld strength mismatch on crack-tip constraint in single edge notch bend specimens, *International Journal of Fracture* 63 (1993) 297-316.
- [6] X. K. Zhu, Y. J. Chao, Fully plastic crack-tip fields for CCP and DECP specimens under tension in non-hardening materials, *International Journal of Solids and Structures* 37 (2000) 577-598.
- [7] G.H. Paulino, J.H. Kim, A new approach to compute T -stress in functionally graded materials by means of the interaction integral method, *Engineering Fracture Mechanics* 71 (2004) 1907-1950.
- [8] N.P. O'Dowd, C.F. Shih, R.H. Dodds, The role of geometry and crack growth on constraint and implications for ductile/brittle fracture, in: M. Kirk, A. Bakker (Eds.), STP1244, *Constraint effects in fracture theory and applications*, Second volume, Philadelphia, American Society for Testing and Materials 1995, pp.134-159.
- [9] J.D.G. Sumpter, An experimental investigation of the T stress approach, in: E.M. Hackett (Eds.), STP 1171, *Constraint Effects in Fracture*, American Society for Testing and Materials, 1993, pp. 495-502.
- [10] J.N. Masters, W.P. Haese, R.W. Finger, Investigation of deep flaws in thin walled tanks, NASA CR-72606, The Boeing Company, Seattle, Wash., Dec, 1969.
- [11] M. Gupta, R.C. Alderliesten, R. Benedictus, A review of T-stress and its effects in fracture mechanics, *Engineering Fracture Mechanics* (2014), in press, <<http://dx.doi.org/10.1016/j.engfracmech.2014.1010.1013>>.
- [12] G.E. Cardew, M.R. Goldthorpe, I.C. Howard, A.P. Kfoury, On the Elastic T -term, in: B.A. Bibby, K.J. Miller, J.R. Willis (Eds.), *Fundamentals of Deformation and Fracture*, Cambridge: Cambridge University Press, 1984, pp. 465-476.
- [13] A.P. Kfoury, Some evaluations of the elastic T-term using Eshelby's method, *International Journal of Fracture* 30 (1986) 301-315.
- [14] T. Nakamura, D.M. Parks, Determination of elastic T -stress along three-dimensional crack fronts using an interaction integral, *International Journal of Solids and Structures* 29 (1992) 1597-1611.
- [15] A.H. Sherry, C.C. France, M.R. Goldthorpe, Compendium of t-stress solutions for two and three dimensional cracked geometries, *Fatigue & Fracture of Engineering Materials & Structures* 18 (1995)

141-155.

[16] T. Fett, T-stresses in rectangular plates and circular disks, *Engineering Fracture Mechanics* 60 (1998) 631-652.

[17] X. Wang, Elastic T-stress for cracks in test specimens subjected to non-uniform stress distributions, *Engineering Fracture Mechanics* 69 (2002) 1339-1352.

[18] X. Wang, R. Bell, Elastic T -stress solutions for semi-elliptical surface cracks in finite thickness plates subject to non-uniform stress distributions, *Engineering Fracture Mechanics* 71 (2004) 1477-1496.

[19] V.N. Shlyannikov, T -stress for crack paths in test specimens subject to mixed mode loading, *Engineering Fracture Mechanics* 108 (2013) 3-18.

[20] Y.G. Matvienko, V.N. Shlyannikov, N.V. Boychenko, In-plane and out-of-plane constraint parameters along a three-dimensional crack-front stress field under creep loading, *Fatigue & Fracture of Engineering Materials & Structures* 36 (2013) 14-24.

[21] V.N. Shlyannikov, N.V. Boychenko, A.V. Tumanov, A. Fernández-Canteli, The elastic and plastic constraint parameters for three-dimensional problems, *Engineering Fracture Mechanics* 127 (2014) 83-96.

[22] C.L. Tan, X. Wang, The use of quarter-point crack-tip elements for T -stress determination in boundary element method analysis, *Engineering Fracture Mechanics* 70 (2003) 2247-2252.

[23] C.H. Chen, C.L. Wang, Stress intensity factors and T -stresses for offset double edge-cracked plates under mixed-mode loadings, *International Journal of Fracture* 152 (2008) 149-162.

[24] B.S. Henry, A.R. Luxmoore, Three-dimensional evaluation of the T-stress in centre cracked plates, *International Journal of Fracture* 70 (1994) 35-50.

[25] M. R. Ayatollahi, M.R.M. Aliha., Analysis of a new specimen for mixed mode fracture tests on brittle materials, *Engineering Fracture Mechanics* 76 (2009) 1563-1573.

[26] V.F. González-Albuixech, E. Giner, J. Fernández-Sáez, A. Fernández-Canteli, Influence of the T_{33} -stress on the 3-D stress state around corner cracks in an elastic plate, *Engineering Fracture Mechanics* 78 (2011) 412-427.

[27] T. Meshii, K. Lu, R. Takamura, A failure criterion to explain the test specimen thickness effect on fracture toughness in the transition temperature region, *Engineering Fracture Mechanics* 104 (2013) 184-197.

[28] K. Lu, T. Meshii, Three-dimensional T -stresses for three-point-bend specimens with large thickness variation, *Engineering Fracture Mechanics* 116 (2014) 197-203.

[29] K. Lu, T. Meshii, Application of T_{33} -Stress to Predict the Lower Bound Fracture Toughness for Increasing the Test Specimen Thickness in the Transition Temperature Region, *Advances in Materials Science and Engineering* (2014) <<http://dx.doi.org/10.1155/2014/269137>>.

[30] T. Meshii, K. Lu, Y. Fujiwara, Extended investigation of the test specimen thickness (TST) effect on the fracture toughness (J_c) of a material in the ductile-to-brittle transition temperature region as a difference in the crack tip constraint – What is the loss of constraint in the TST effects on J_c ?,

Engineering Fracture Mechanics (2014), in press,
<<http://dx.doi.org/10.1016/j.engfracmech.2014.1007.1025>>.

[31] T. Meshii, T. Tanaka, K. Lu, *T*-Stress solutions for a semi-elliptical axial surface crack in a cylinder subjected to mode-I non-uniform stress distributions, *Engineering Fracture Mechanics* 77 (2010) 2467-2478.

[32] T. Meshii, T. Tanaka, Experimental T_{33} -stress formulation of test specimen thickness effect on fracture toughness in the transition temperature region, *Engineering Fracture Mechanics* 77 (2010) 867-877.

[33] ASTM, E2472-06 standard test method for determination of resistance to stable crack extension under low-constraint conditions, Annual book of ASTM standards, 2006.

[34] M.L. Williams, On the stress distribution at the base of a stationary crack, *Journal of Applied Mechanics* 24 (1957) 111-114.

[35] M. Isida, Effect of width and length on stress intensity factors of internally cracked plates under various boundary conditions, *International Journal of Fracture Mechanics* 7 (1971) 301-316.

[36] Z. Wu, On the through-thickness crack with a curve front in center-cracked tension specimens, *Engineering Fracture Mechanics* 73 (2006) 2600-2613.

[37] J.C. Newman Jr, M. Jordan Haines, Verification of stress-intensity factors for various middle-crack tension test specimens, *Engineering Fracture Mechanics* 72 (2005) 1113-1118.

[38] Quest Integrity Group, 3D finite element software for cracks: Version 3.2 user's manual, Boulder, CO80301, USA, 2013.

[39] B. Healy, A. Gullerud, K. Koppenhoefer, A. Roy, S. RoyChowdhury, J. Petti, M. Walters, B. Bichon, K. Cochran, A. Carlyle, J. Sobotka, M. Messner, R.H. Dodds, WARP3D Release 17.5.3 Manual, Civil Engineering, Report No UIUC-ENG-95-2012, University of Illinois at Urbana-Champaign, 2014.

[40] J. Heerens, U. Zerbst, K.H. Schwalbe, Strategy for characterizing fracture toughness in the ductile to brittle transition regime, *Fatigue & Fracture of Engineering Materials & Structures* 16 (1993) 1213-1230.

[41] A. Fernández-Canteli, E. Giner, J. Fernández-Sáez, D. Fernández-Zúñiga, A unified analysis of the in-plane and out-of-plane constraints in 3-D linear elastic fracture toughness, *Proceedings of the 19th European Conference on Fracture*, Kazan, Russia, 2012, pp.1-8.

Table 1 Comparisons of the mid-plane normalized T -stress results for CCT specimens from the present FEA and the superposition method ($2W = 300$ mm, $H/W = 2$, $B/(2W) = 1.0$; $\nu = 0.3$)

a/W	0.05	0.1	0.15	0.2	0.3	0.4	0.5	0.6	0.7	0.8
V_{11} Kfourri	(-)	-0.995	(-)	-1.028	-1.076	-1.136	-1.219	-1.350	(-)	(-)
V_{11}	-1.003	-1.010	-1.022	-1.039	-1.090	-1.166	-1.285	-1.479	-1.827	-2.566
$ V_{11} - V_{11} \text{ Kfourri} / V_{11} \text{ Kfourri} \times 100\%$	(-)	1.5	(-)	1.1	1.3	2.6	5.4	9.5	(-)	(-)
$V_{11} \text{ sup}$	-1.003	-1.010	-1.022	-1.039	-1.090	-1.166	-1.285	-1.479	-1.827	-2.566
$ V_{11} - V_{11} \text{ sup} / V_{11} \text{ sup} \times 100\%$	0.02	0	0.02	0.03	0.01	0.02	0.01	0.01	0	0
V_{33}	-0.5989	-0.5953	-0.5899	-0.5837	-0.5762	-0.5826	-0.6183	-0.6930	-0.8407	-1.124
$V_{33} \text{ sup}$	-0.5988	-0.5953	-0.5899	-0.5838	-0.5758	-0.5831	-0.6175	-0.6941	-0.8401	-1.124
$ V_{33} - V_{33} \text{ sup} / V_{33} \text{ sup} \times 100\%$	0.01	0	0.01	0.03	0.07	0.09	0.13	0.16	0.07	0.02

*(-): no result exists for comparison

Table 2 Normalized T_{11} solutions ($V_{11} = T_{11}/\sigma$) at the specimen mid-plane for CCT specimens ($\nu = 0.3$)

a/W $B/(2W)$	0.05	0.1	0.15	0.2	0.3	0.4	0.5	0.6	0.7	0.8
0.01	-0.9142	-0.8811	-0.8600	-0.8468	-0.8402	-0.8612	-0.9207	-1.046	-1.306	-1.906
0.025	-0.9487	-0.9290	-0.9190	-0.9156	-0.9268	-0.9660	-1.046	-1.197	-1.491	-2.146
0.0625	-0.9920	-0.9616	-0.9567	-0.9593	-0.9819	-1.032	-1.125	-1.291	-1.606	-2.288
0.1	-1.012	-0.9842	-0.9730	-0.9756	-1.002	-1.056	-1.153	-1.324	-1.643	-2.328
0.25	-1.009	-1.020	-1.020	-1.019	-1.036	-1.090	-1.189	-1.365	-1.698	-2.457
0.5	-1.004	-1.014	-1.028	-1.042	-1.075	-1.131	-1.234	-1.425	-1.791	-2.564
1.0	-1.003	-1.010	-1.022	-1.039	-1.090	-1.166	-1.285	-1.479	-1.827	-2.566

Table 3 Normalized T_{33} solutions ($V_{33} = T_{33}/\sigma$) at the specimen mid-plane for CCT specimens ($\nu = 0.3$)

a/W $B/(2W)$	0.05	0.1	0.15	0.2	0.3	0.4	0.5	0.6	0.7	0.8
0.01	-1.048	-1.453	-1.778	-2.067	-2.600	-3.142	-3.758	-4.516	-5.562	-7.267
0.025	-0.7086	-0.9522	-1.152	-1.331	-1.666	-2.008	-2.394	-2.872	-3.537	-4.599
0.0625	-0.5272	-0.6529	-0.7718	-0.8811	-1.086	-1.301	-1.543	-1.848	-2.270	-2.952
0.1	-0.5169	-0.5568	-0.6422	-0.7253	-0.8836	-1.050	-1.242	-1.483	-1.816	-2.346
0.25	-0.5721	-0.5305	-0.5203	-0.5385	-0.6198	-0.7203	-0.8388	-0.9882	-1.193	-1.537
0.5	-0.5929	-0.5744	-0.5539	-0.5392	-0.5409	-0.5803	-0.6504	-0.7571	-0.9411	-1.317
1.0	-0.5989	-0.5953	-0.5899	-0.5837	-0.5762	-0.5826	-0.6183	-0.6930	-0.8407	-1.124

Table A.1 Summary of the detailed mesh generation (NE: number of elements)

$B/(2W)$	a/W	0.05	0.1	0.15	0.2	0.3	0.4	0.5	0.6	0.7	0.8
0.01	$\Delta a \times 10^3$	6.7	3.3	2.2	1.7	1.1	0.83	0.67	0.56	0.48	0.42
	NE of CD	3	5	7	8	15	20	24	28	32	38
	NE of NR	41	41	39	36	31	29	26	21	16	10
	NE of na (bias)	90(2)									
0.025	$\Delta a \times 10^3$	6.7	3.3	2.2	1.7	1.1	0.83	0.67	0.56	0.48	0.42
	NE of CD	3	5	7	8	15	20	24	28	32	38
	NE of NR	42	42	40	38	32	30	24	20	14	8
	NE of na (bias)	90(2)									
0.0625	$\Delta a \times 10^3$	6.7	3.3	2.2	1.7	1.1	0.83	0.67	0.56	0.48	0.42
	NE of CD	3	5	7	8	15	20	24	28	32	38
	NE of NR	43	43	41	39	33	31	25	21	16	10
	NE of na (bias)	90(2)									
0.1	$\Delta a \times 10^3$	6.7	3.3	2.2	1.7	1.1	0.83	0.67	0.56	0.48	0.42
	NE of CD	3	5	7	8	15	20	24	28	32	38
	NE of NR	40	40	38	35	35	27	23	20	16	11
	NE of na (bias)	90(2)									
0.25	$\Delta a \times 10^3$	6.7	3.3	2.2	1.7	1.1	0.83	0.67	0.56	0.48	0.42
	NE of CD	4	5	7	8	15	20	24	28	32	38
	NE of NR	51	49	47	34	36	28	22	21	16	10
	NE of na (bias)	135 (2)									
0.5	$\Delta a \times 10^3$	6.7	3.3	2.2	1.7	1.1	0.83	0.67	0.56	0.48	0.42
	NE of CD	4	5	7	8	15	20	24	28	32	38
	NE of NR	54	49	46	44	36	25	24	20	16	10
	NE of na (bias)	135 (2)									
1.0	$\Delta a \times 10^3$	6.7	3.3	2.2	1.7	1.1	0.83	0.67	0.56	0.48	0.42
	NE of CD	4	6	7	8	15	20	24	25	32	38
	NE of NR	40	40	40	40	36	25	24	20	16	10
	NE of na (bias)	189 (2)									

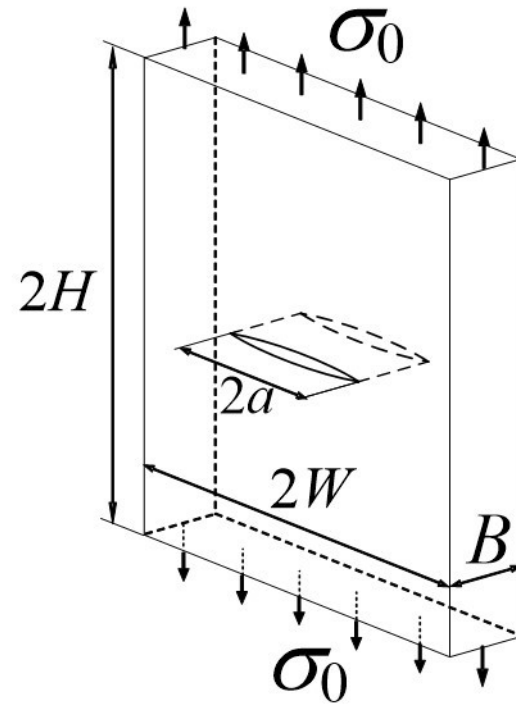


Fig. 1 CCT specimen

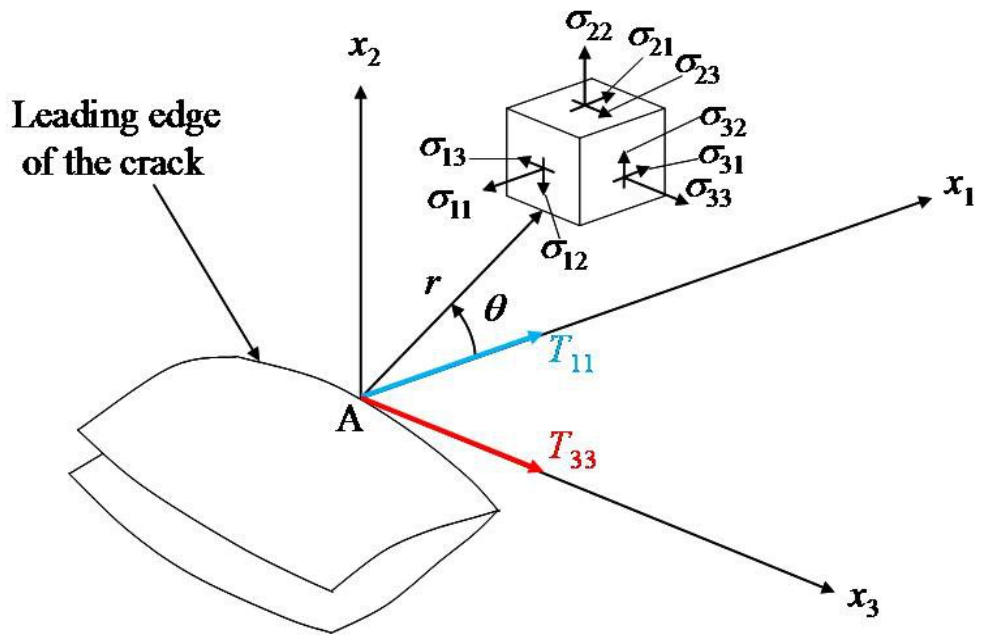


Fig. 2 Three-dimensional coordinate system for the region along the crack front [28, 32]

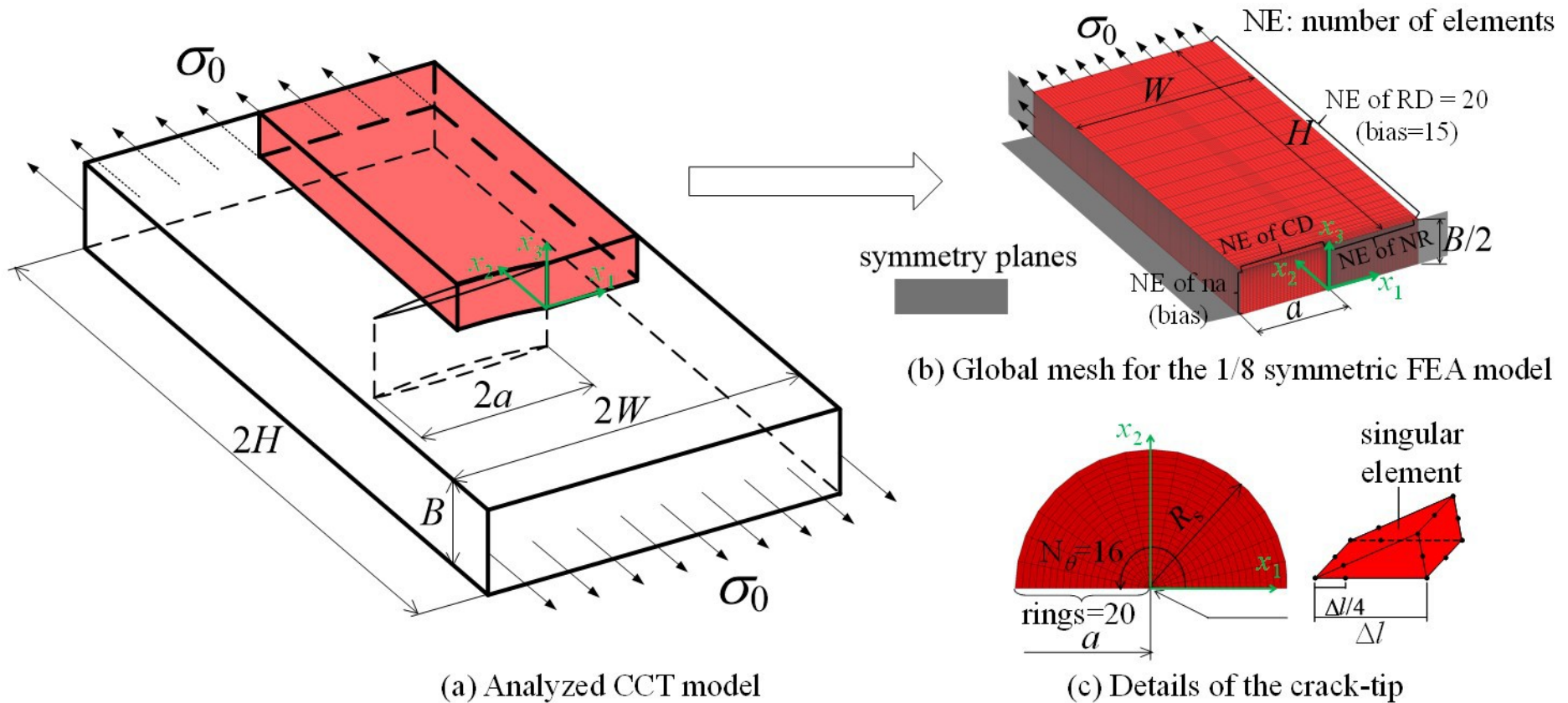


Fig. 3. Typical 1/8 symmetric finite element model of a CCT specimen ($2W = 300$ mm, $H/W = 2$, $B/(2W) = 0.5$ and $a/W = 0.5$). Note that the detailed information for the mesh generation parameters (Δl , CD, NR and na) is summarized in the Appendix.

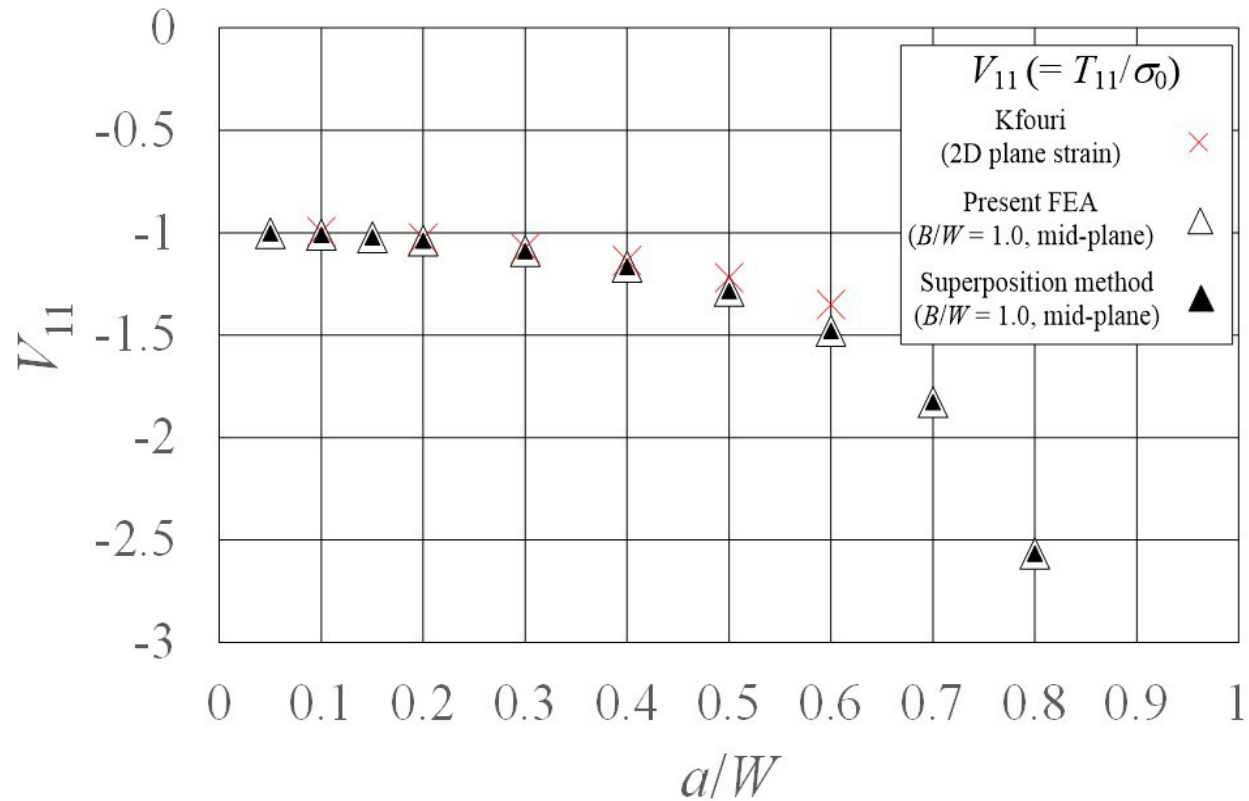


Fig. 4 Comparison of the normalized 3D mid-plane T_{11} solutions ($V_{11} = T_{11}/\sigma_0$) with Kfouri's 2D plane strain solutions [13] and the solutions from the superposition method for the CCT specimens with $B/(2W) = 1.0$ ($\nu = 0.3$)

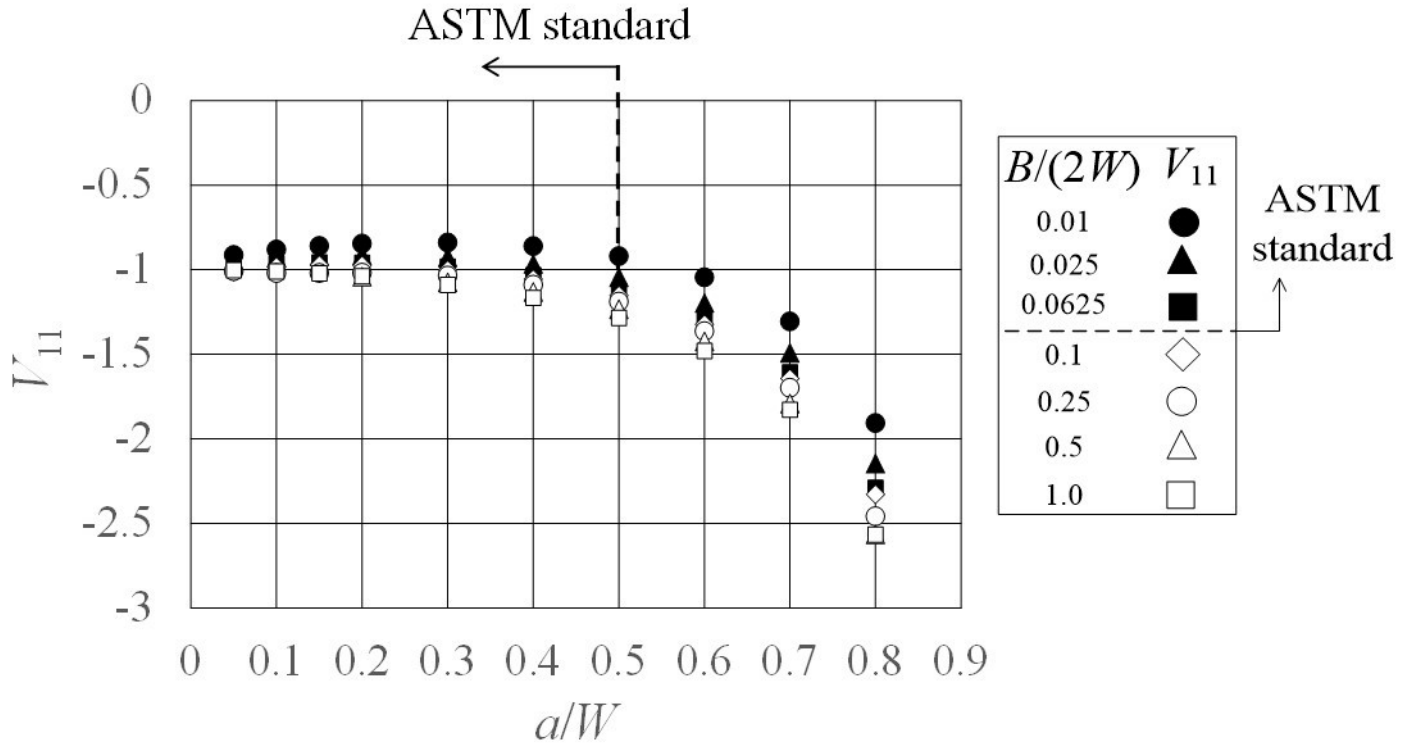


Fig. 5 Normalized T_{11} solutions ($V_{11} = T_{11}/\sigma_0$) at the specimen mid-plane for CCT specimens ($\nu = 0.3$)

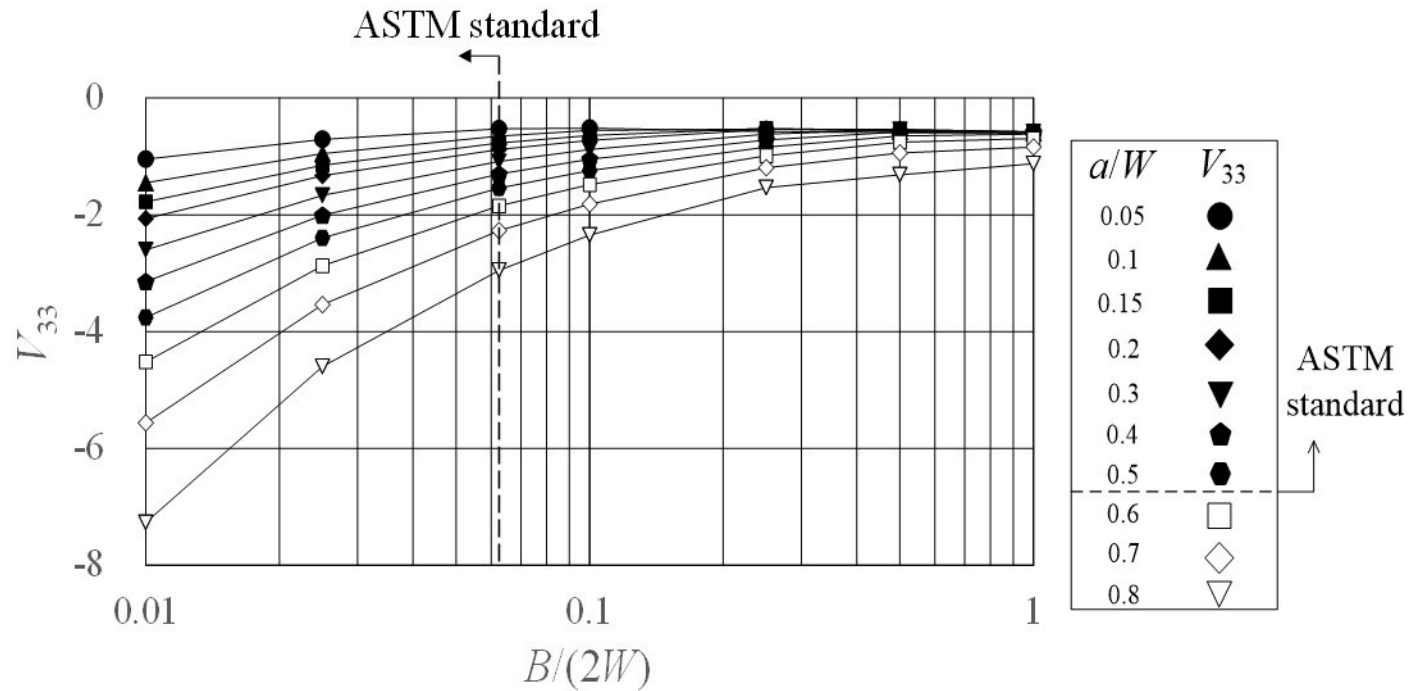


Fig. 6 Normalized T_{33} solutions ($V_{33} = T_{33}/\sigma_0$) at the specimen mid-plane for CCT specimens ($\nu = 0.3$)

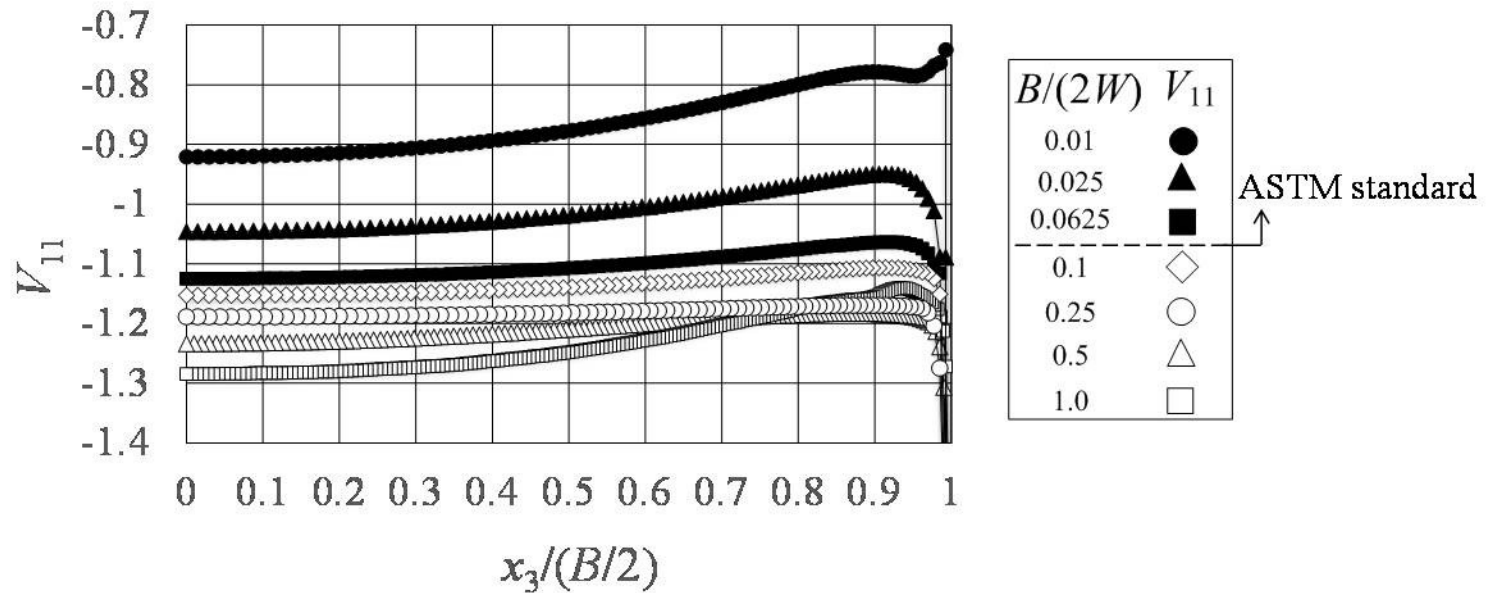


Fig. 7 Normalized T_{11} solutions ($V_{11} = T_{11}/\sigma_0$) vs. $x_3/(B/2)$ for the CCT specimens with various thicknesses ($a/W = 0.5$; $\nu = 0.3$)

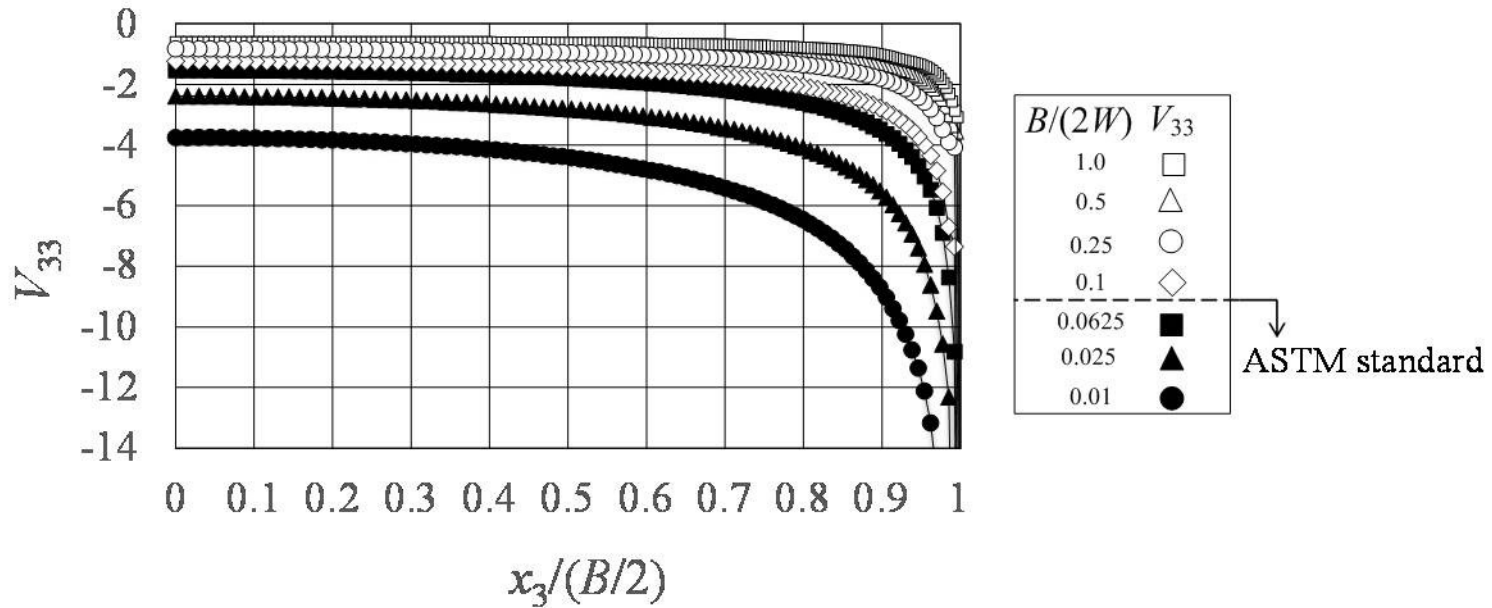


Fig. 8 Normalized T_{33} solutions ($V_{33} = T_{33}/\sigma_0$) vs. $x_3/(B/2)$ for the CCT specimens with various thicknesses ($a/W = 0.5$; $\nu = 0.3$)

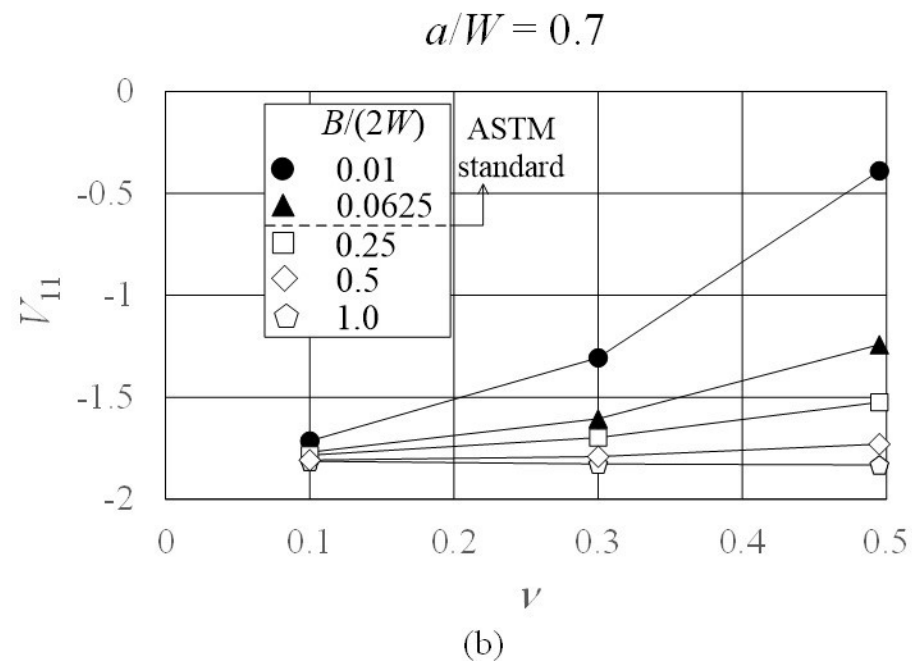
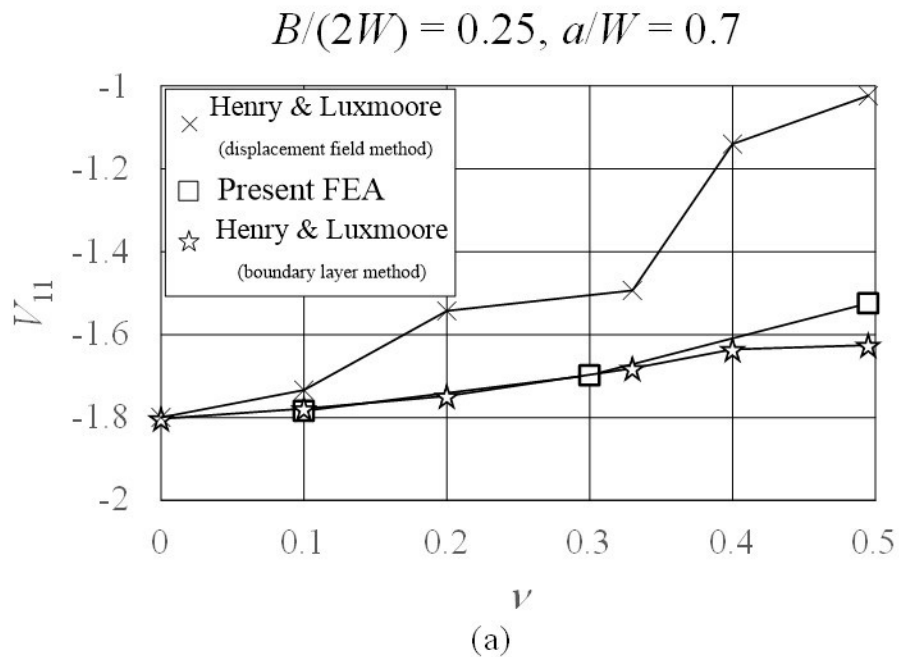
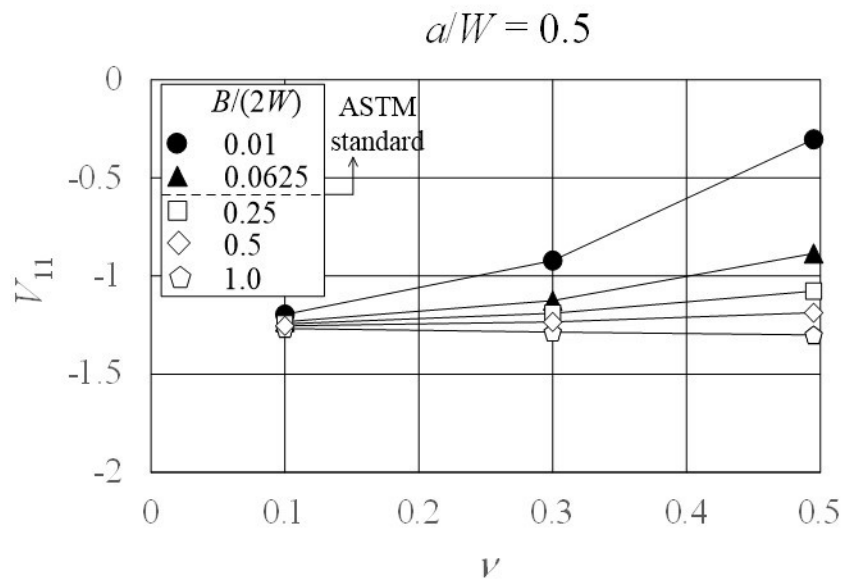
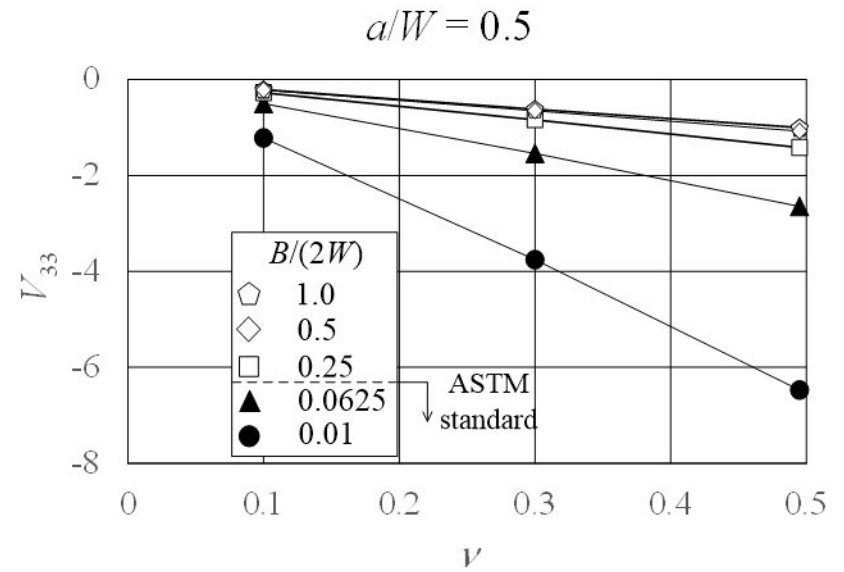


Fig. 9 Effects of Poisson's ratio ν on the mid-plane V_{11} for the case of $a/W = 0.7$: (a) comparison of present V_{11} for $B/(2W) = 0.25$ with Henry and Luxmoore's results [24] (b) present V_{11} for various thicknesses



(a) The mid-plane V_{11} vs. Poisson's ratio ν



(b) The mid-plane V_{33} vs. Poisson's ratio ν

Fig. 10 Effects of Poisson's ratio ν on the mid-plane V_{11} and V_{33} for a case of $a/W = 0.5$: (a) V_{11} vs. ν , (b) V_{33} vs. ν

Highlights

1. T -stresses for CCT specimens with various crack lengths and thicknesses were obtained.
2. T_{11} and T_{33} were negative for all of the CCT specimens studied in this work.
3. Both T_{11} and T_{33} changed significantly for the ASTM E2472 standard CCT specimens.